Research Square

Preprints are preliminary reports that have not undergone peer review.
They should not be considered conclusive, used to inform clinical practice,
or referenced by the media as validated information.

Green Synthesis of Silver Nanoparticles Using Tagetes erecta Flower Extract: Structural Characterization and Dose-Dependent Antifungal Efficacy Against Fusarium oxysporum and Rhizoctonia solani of chickpea

Pooja Parmar
Jawaharlal Nehru Krishi Vishwa Vidyalaya
Ashish Kumar
Jawaharlal Nehru Krishi Vishwa Vidyalaya
Vedant Gautam
vedantgautam@bhu.ac.in

Jawaharlal Nehru Krishi Vishwa Vidyalaya
Radheshyam Sharma
Jawaharlal Nehru Krishi Vishwa Vidyalaya
Anurag Chouhan
Jawaharlal Nehru Krishi Vishwa Vidyalaya

Research Article

Keywords: Phytosynthesis, Nanofungicide, Sustainable disease management, JG322, chickpea

Posted Date: September 2nd, 2026

DOI: https://doi.org/10.21203/rs.3.rs-10624775/v1

License: This work is licensed under a Creative Commons Attribution 4.0 International License.
Read Full License

Additional Declarations: No competing interests reported.

Green Synthesis of Silver Nanoparticles Using *Tagetes erecta* Flower Extract: Structural Characterization and Dose-Dependent Antifungal Efficacy Against *Fusarium oxysporum* and *Rhizoctonia solani* of chickpea

Pooja Parmar[1], Ashish Kumar[1,*], Vedant Gautam[1,*], Radheshyam Sharma[2], Anurag Chouhan[1]

[1]Department of Plant Pathology, Jawaharlal Nehru Krishi Vishwavidyalaya, Jabalpur, Madhya Pradesh, 482004, India

[2]Department of Plant Biotechnology, Jawaharlal Nehru Krishi Vishwavidyalaya, Jabalpur, Madhya Pradesh, 482004, India

Corresponding Author:

Vedant Gautam (vedantgautam@bhu.ac.in), Orcid id- https://orcid.org/0000-0002-0103-1947

Ashish Kumar (ashishkumar@jnkvv.org)

Abstract

Silver nanoparticles (AgNPs) were green-synthesized using aqueous *Tagetes erecta* (marigold) flower extract as a reducing and capping agent, and evaluated for antifungal efficacy against *Fusarium oxysporum* and *Rhizoctonia solani* under in vitro and in vivo conditions. X-ray diffraction confirmed the crystalline, face-centred cubic structure of metallic Ag, with characteristic peaks at 2θ = 38.1°, 46.2°, and additional reflections at 27.8°, 32.2°, 54.8°, and 57.4° attributable to a minor AgCl phase; the average crystallite size, calculated using the Debye–Scherrer equation, was 19 nm. SEM and TEM analyses revealed predominantly spherical to quasi-spherical, polydisperse nanoparticles (~20 nm range) embedded within an organic phytoconstituent matrix, consistent with biomolecule-mediated capping. In vitro, AgNPs exhibited dose-dependent inhibition of mycelial growth, reducing *F. oxysporum* radial growth by 31.89%, 48.76%, and 69.27% at 50, 100, and 200 ppm, respectively, and *R. solani* growth by 41.49%, 60.67%, and 77.04% at the same concentrations, compared to 85.04% and 91.51% inhibition by azoxystrobin (100 ppm) against the two pathogens. Under pot culture conditions, 200 ppm AgNPs reduced Fusarium wilt and Rhizoctonia root rot severity by 64.9% and 72.3%, respectively, statistically on par with azoxystrobin at 80 ppm (68.4% and 75.0% reduction), while azoxystrobin at 100 ppm remained the most effective treatment overall (84.4% and 86.4% reduction). These findings demonstrate that *T. erecta*-mediated AgNPs possess strong, concentration-dependent antifungal activity approaching fungicide-equivalent efficacy at 200 ppm, positioning them as a promising eco-friendly alternative for integrated management of soil-borne fungal pathogens.

Keywords: Phytosynthesis, Nanofungicide, Sustainable disease management, JG322, chickpea.

1 Introduction

Chickpea (*Cicer arietinum* L.) is among the most economically important pulse crops of the semi-arid tropics, but its productivity is severely constrained by soil-borne fungal diseases, chief among them Fusarium wilt, caused by *Fusarium oxysporum* f. sp. *ciceris*, and root rot, caused by *Rhizoctonia solani*. Field epidemiological studies conducted over multiple seasons and chickpea cultivars have shown that Fusarium wilt reduces both seed yield and seed weight, with the extent of loss governed by sowing date, cultivar susceptibility, and the virulence of the prevailing pathogen race [1]. Yield losses from wilt have been reported to range from about 10% in normal years to as high as 70–100% during severe epidemics, and root rot pathogens are similarly capable of causing substantial yield reduction, particularly under favourable soil moisture and temperature conditions. Both pathogens frequently co-occur in the same field, complicating diagnosis and integrated management.

Management of these diseases has traditionally relied on synthetic fungicides, resistant cultivars, and cultural practices. Among fungicides, strobilurins such as azoxystrobin remain widely used owing to their broad-spectrum efficacy against soil-borne pathogens; however, repeated and prolonged use of single-mode-of-action fungicides raises concerns over resistance development, non-target toxicity, and residue accumulation, prompting the search for safer, sustainable alternatives that can complement or reduce dependence on conventional chemistries.

Nanotechnology has recently emerged as a promising frontier in plant disease management, with metal and metal-oxide nanoparticles receiving considerable attention for their broad-spectrum antimicrobial and pesticidal properties. Silver nanoparticles (AgNPs) are known to disrupt fungal cell walls and membranes, generate reactive oxygen species, and interfere with protein and DNA function, mechanisms that collectively translate into inhibition of mycelial growth and spore germination across a range of phytopathogenic fungi [2]. Beyond antifungal applications, biologically synthesized nanoparticles have also shown promise against other soil-borne crop pests. Fungal-derived zinc oxide nanoparticles functionalized with riboflavin and UDP-N-acetylglucosamine, for instance, recently demonstrated potent nematicidal activity against the root-knot nematode *Meloidogyne incognita* [3]. This broadens the case for biogenic nanoparticle–metabolite composites as multi-target, eco-friendly crop protection agents. Within the antifungal domain specifically, plant-mediated

AgNPs synthesized from extracts such as *Avena fatua* have shown concentration- and exposure-time-dependent efficacy against *Fusarium oxysporum* f. sp. *lycopersici* [4], while AgNPs synthesized using *Solanum nigrum* leaf extract have demonstrated significant inhibition of *Fusarium circinatum* and related pathogens isolated from diseased plant tissue [5].

Among candidate plant sources, marigold (*Tagetes erecta*), an easily cultivated ornamental rich in flavonoids, terpenoids, and phenolic compounds, has been repeatedly and successfully used for AgNP biosynthesis. Aqueous flower extract of *T. erecta* has been shown to reduce silver ions into stable, well-characterized nanoparticles with demonstrable antimicrobial activity [6,7] and comparative studies using aqueous and ethanolic *T. erecta* flower extracts have further optimized synthesis conditions and confirmed nanoscale, spherical particle morphology [8]. More recently, leaf and petal extracts of *T. erecta* have also been used to generate long-lasting AgNPs with confirmed antibacterial efficacy against agronomically important pathogens [9], underscoring the versatility of this plant as a green synthesis matrix.

Despite this growing body of literature on AgNP synthesis and general antimicrobial screening, comparative data on the efficacy of marigold-derived AgNPs against major chickpea soil-borne pathogens—*F. oxysporum* f. sp. *ciceris* and *R. solani*—under both in vitro and in vivo conditions, benchmarked against a standard fungicide, remain limited. The present study was therefore undertaken to green-synthesize and characterize AgNPs using *Tagetes erecta* flower extract, and to evaluate their dose-dependent antifungal efficacy against these two pathogens in vitro and under pot conditions, in comparison with azoxystrobin, with a view to assessing their potential as a sustainable component of integrated disease management in chickpea.

2 Materials and Methods

2.1 Plant Material and Preparation of the Extract

For the preparation of plant extract, fresh flowers of *Tagetes erecta* were collected and thoroughly washed with tap water followed by double distilled water to remove dust and contaminants. Approximately 10 g of sterilized flower material was chopped into small pieces and transferred into a beaker containing 200 ml of ultrapure water. The mixture was boiled on a hot plate for 10 min. The boiled solution was allowed to cool at room temperature and then filtered through Whatman filter paper No. 1 to obtain a clear plant extract.

2.2 Preparation of Leaf Extract

Fresh, healthy flowers of *Tagetes erecta* were thoroughly washed with running tap water followed by distilled water to remove dust and other adhering impurities. The cleaned flowers were cut into small pieces, and 5 g of the fresh floral tissue was added to 100 mL of ultrapure (or distilled) water in a 250 mL Erlenmeyer (conical) flask. The mixture was boiled for 10 min and allowed to cool to room temperature. The extract was filtered through Whatman No. 1 filter paper to remove residual plant material. The clear filtrate was collected and stored at 4 °C until further use as the reducing and stabilizing agent for the green synthesis of silver nanoparticles.

2.3 Green Synthesis of Silver Nanoparticles (AgNPs)

A 1 mM silver nitrate ($AgNO_3$) solution was prepared by dissolving 0.168 g of $AgNO_3$ in 1000 ml of distilled water in an amber conical flask to maintain dark conditions because of the photosensitive nature of $AgNO_3$. During preliminary standardization experiments, 15% (v/v) plant extract was found suitable for nanoparticle synthesis. Therefore, 150 ml of plant extract was mixed with 850 ml of 1 mM $AgNO_3$ solution. The reaction mixture was incubated in an amber container at room temperature for 24 h for the reduction of Ag^+ ions. A visible change in the colour of the solution from transparent to brown indicated the formation of silver nanoparticles (Figure 1). After completion of the reduction process, the reaction mixture was centrifuged at 10,000 rpm for 10 min. The obtained pellet containing AgNPs was washed repeatedly with Milli-Q water to remove impurities. The purified nanoparticles were redispersed in deionized water and stored in dark conditions for further analysis.

2.4 X-ray Diffraction (XRD) Analysis

The purified AgNPs suspension was repeatedly centrifuged and the obtained pellet was dried to obtain nanoparticle powder. The crystalline structure and composition of the synthesized AgNPs were analyzed using an X-ray diffractometer (PANalytical BV, The Netherlands) operated at 40 kV and 30 mA with Cu Kα radiation in θ–2θ configuration [10].

The crystallite size of AgNPs was calculated using the Scherrer equation:

$$D = \frac{0.94\lambda}{\beta \cos\theta}$$

where D is the crystallite size, λ is the wavelength of X-ray radiation, β is the full width at half maximum (FWHM), and θ is the diffraction angle.

2.5 Scanning Electron Microscopy (SEM) Analysis

Surface morphology of the biosynthesized AgNPs was examined using a scanning electron microscope (Quanta 200, Thermo fisher) operated at an accelerating voltage of 20 kV. A small amount of the dried nanoparticle sample was mounted on a carbon tape and sputter-coated with gold under vacuum to enhance surface conductivity prior to imaging. Micrographs were captured at multiple magnifications (2,000×, 10,000×, 50,000×).

2.6 Transmission Electron Microscopy (TEM) Analysis

The size, shape, and dispersity of the AgNPs were examined using a transmission electron microscope (Model: Tecnai 20 G2, Thermo fisher) operated at an accelerating voltage of 100 kV. A drop of the well-sonicated aqueous nanoparticle suspension was placed onto a carbon-coated copper grid (300 mesh) and allowed to air-dry at room temperature before imaging. Particle size distribution was assessed manually/using (ImageJ) software against the embedded scale marker.

2.7 Fungal Pathogen Cultures

Pure cultures of *Fusarium oxysporum* f. sp. *ciceris*, of chickpea wilt isolate and *Rhizoctonia solani* were obtained from infected plant samples at Department of Plant Pathology, JNKVV. Cultures were maintained and sub-cultured on potato dextrose agar (PDA) medium at 25 ± 2 °C and periodically revived prior to use in bioassays.

2.8 In Vitro Antifungal Bioassay (Poisoned Food Technique)

The antifungal activity of AgNPs against *F. oxysporum* and *R. solani* was evaluated in vitro by the poisoned food technique. AgNP stock suspension was incorporated into molten, sterilized PDA medium to achieve final concentrations of 50, 100, and 200 ppm. The amended medium was poured into sterile Petri plates (90 mm diameter) and allowed to solidify. A 5 mm mycelial disc, cut from the actively growing margin of a 7-day-old pathogen culture, was placed at the centre of each plate. Plates without AgNP amendment served as the pathogen control (T2), and un-inoculated PDA plates served as the healthy control (T1). Standard fungicide checks were prepared using azoxystrobin at 80 ppm (T6) and 100 ppm (T7) incorporated into PDA in the same manner. All plates were incubated at 25 ± 2 °C in the dark and radial mycelial growth was recorded at 3, 5 and 7 days after inoculation (DAI) using a ruler. Each treatment was replicated 5 times in a completely randomized design (CRD). Per cent mycelial growth inhibition (PGI) was calculated using the formula:

$$\text{PGI}\ (\%) = \frac{(\text{C} - \text{T})}{\text{C}} \times 100$$

where C = radial growth of the pathogen in the control, and T = radial growth in the treatment.

2.9 In Vivo Pot Culture Experiment

The protective efficacy of AgNPs was evaluated under pot culture (Net-house) conditions against Fusarium wilt and Rhizoctonia root rot. Chickpea seeds of variety JG 322 were surface-sterilized with 1% NaOCl for 1 minute and rinsed with sterile distilled water. Pots (size: 15*7.5 cm), filled with 1 kg of sterilized soil-sand mixture in the ratio (2:1) were used for the experiment. Pathogen inoculum (10 g of sorghum grown inoculum per kg soil) of *F. oxysporum* and *R. solani* was mixed into the soil 3 days before sowing. Seeds were treated with AgNPs at 50, 100, and 200 ppm by seed soaking for 90 minutes prior to sowing. Azoxystrobin-treated (80 and 100 ppm) and untreated pathogen-inoculated and healthy (un-inoculated) controls were maintained alongside. Pots were arranged in a completely randomized design (CRD) with 5 replications per treatment and maintained under nethouse conditions.

Disease severity of Fusarium wilt and dry root rot was assessed using the 1–9 disease rating scale described by Nene et al. (1981) [11]. A score of 1 indicated healthy plants without visible symptoms; 2, very slight yellowing or drooping of lower leaves in Fusarium wilt or slight browning of lateral roots in dry root rot (<10% affected); 3, mild symptoms affecting 11–20% of the plant or root system; 4, moderate symptoms affecting 21–35% of the plant with initial vascular discoloration (Fusarium wilt) or moderate root rot (dry root rot); 5, disease affecting 36–50% of the plant with pronounced wilting and vascular browning or root decay; 6, severe symptoms affecting 51–65% of the plant with extensive vascular discoloration or collar/root rot; 7, very severe disease affecting 66–80% of the plant with extensive wilting, drying, and root destruction; 8, nearly complete plant collapse affecting 81–90% of the plant; and 9, complete wilting or root rot resulting in plant death (>90% affected). Disease severity was expressed as Percent Disease Index (PDI) using the formula:

$$\text{PDI} = \frac{\sum \text{Disease ratings}}{\text{Number of plants observed} \times 9} \times 100$$

following the standard disease assessment procedures described by Nene et al. (1981).

Per cent disease reduction over the pathogen control was calculated as:

$$\text{Disease reduction (\%)} = \frac{(\text{DSC} - \text{DST})}{\text{DSC}} \times 100$$

where DSC = disease severity in the pathogen-only control, and DST = disease severity in the treatment.

2.5 Statistical Analysis

The obtained experimental data were subjected to statistical analysis using Completely Randomized Design (CRD). The significance of differences among treatments was determined using analysis of variance (ANOVA). Treatment means were compared using the critical difference (CD) test at 5% level of significance.

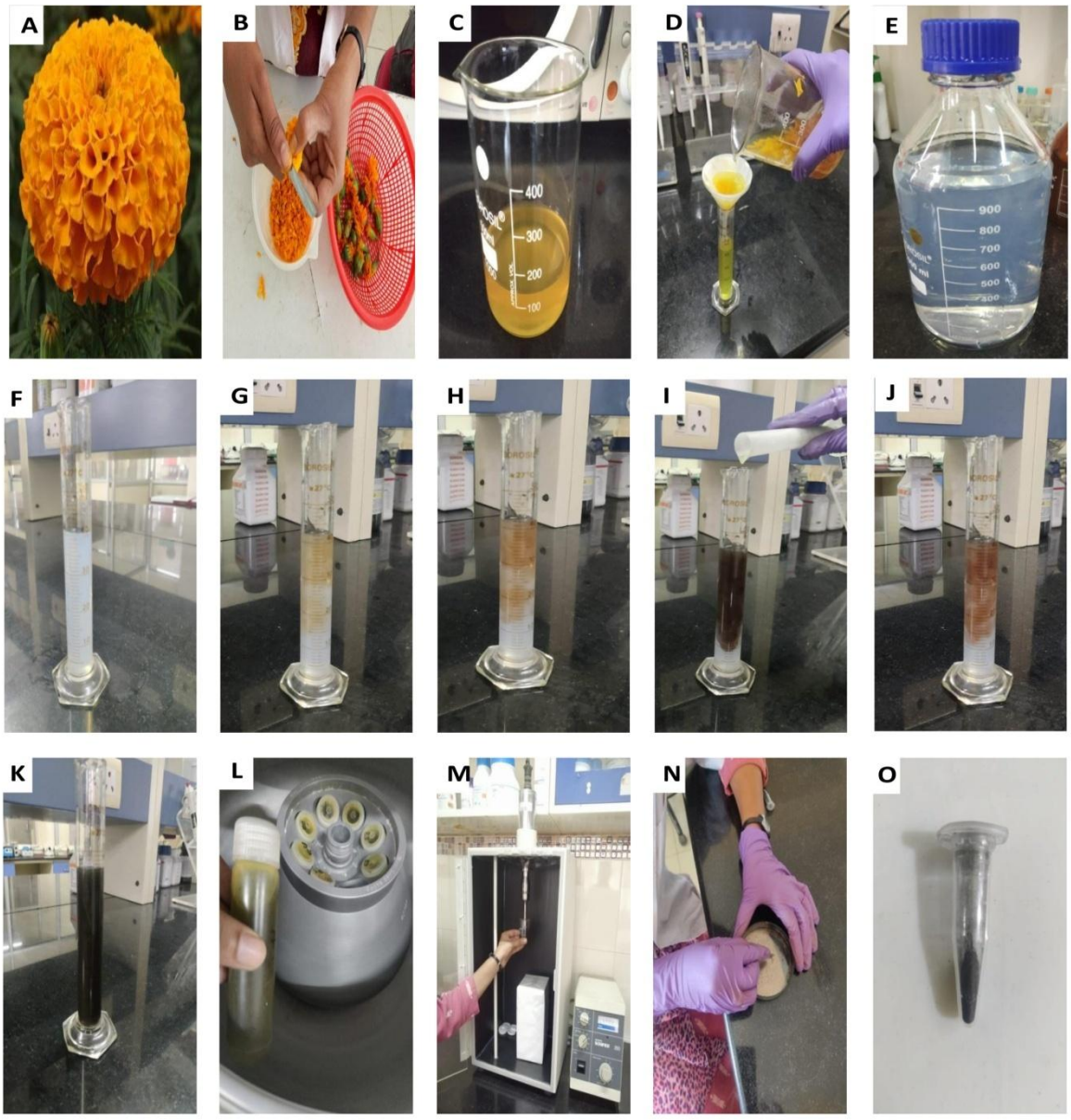


Fig. 1 Green synthesis of silver nanoparticles using marigold flower extract. (A–B) Flower collection and petal separation; (C–E) preparation of aqueous extract and $AgNO_3$ solution; (F–K) time-dependent colour change indicating bio-reduction of Ag^+ to Ag^0; (L–O) centrifugation, washing, and collection of the purified AgNP pellet.

3. Result

3.1 X-ray Diffraction Analysis of Green-Synthesized AgNPs

The crystalline nature of the AgNPs synthesized using *Tagetes erecta* leaf extract was confirmed by XRD analysis (Fig. 2). The diffractogram exhibited several well-resolved Bragg reflections superimposed on a broad background, indicating the presence of nanocrystalline material. Distinct diffraction peaks were recorded at approximately 2θ = 27.8°, 32.2°, 38.1°, 46.2°, 54.8°, 57.4°, 76.7°, and 85.5°.

The peak positions at $2\theta \approx 38.1°$, 44.3°/46.2°, 64.4°, and 77.4° are consistent with the (111), (200), (220), and (311) planes of face-centred cubic (fcc) metallic silver, respectively, in agreement with the standard reference pattern (JCPDS File No. 04-0783). The additional prominent reflections at $2\theta \approx 27.8°$, 32.2°, 54.8°, and 57.4° could not be indexed to metallic Ag and instead correspond closely to the (111), (200), (311), and (222) planes of cubic AgCl (JCPDS File No. 31-1238), suggesting the co-formation of a minor silver chloride phase, most likely arising from chloride ions present in the plant extract reacting with residual Ag^+ during synthesis. The sharp, high-intensity nature of these peaks — most notably the intense reflection near 32.2° — indicates that the synthesized particles are highly crystalline. The mixed Ag/AgCl phase composition observed here is commonly reported in plant-mediated green synthesis of silver nanoparticles, particularly when the extract is rich in chloride-containing phytoconstituents.

The average crystallite size of the synthesized AgNPs, calculated from the full width at half maximum (FWHM) of the most intense diffraction peak using the Debye–Scherrer equation ($D = 0.94\lambda/\beta \cos \theta$), was found to be 21 nm, confirming the nanoscale dimensions of the particles. This is broadly consistent with the size range typically reported for phytosynthesized AgNPs.

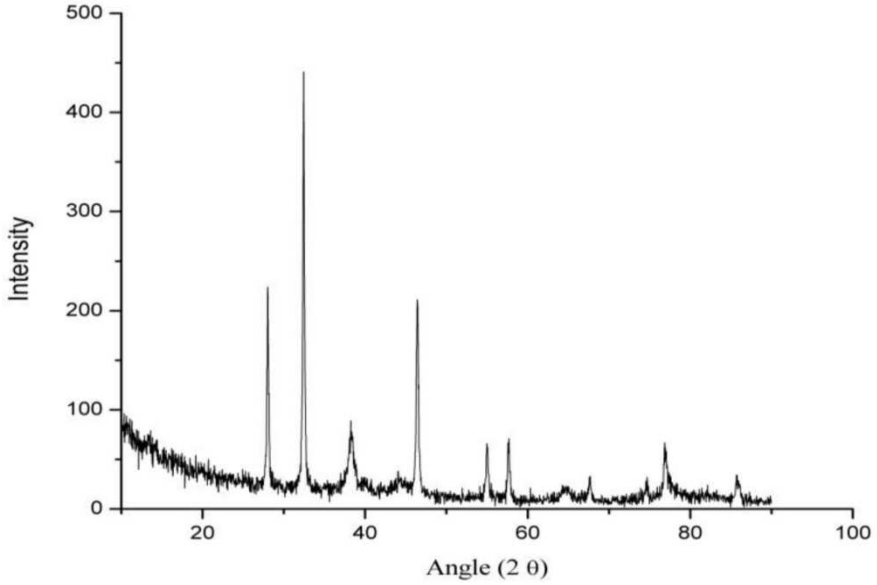


Fig. 2 X-ray diffraction (XRD) pattern of biosynthesized silver nanoparticles. Sharp diffraction peaks observed at 2θ values corresponding to characteristic Bragg reflections confirm the crystalline nature of the synthesized AgNPs, with peak sharpness and intensity indicating good crystallinity of the nanoparticles.

3.2 Scanning Electron Microscopy (SEM) Analysis of AgNPs

The surface morphology of the biosynthesized AgNPs was examined by SEM at varying magnifications (Fig. 3A–D). At higher magnification (50,000×; Fig. 4A), the sample surface appeared as a fine, granular matrix embedded with discrete bright particulate structures of sub-micron dimension, consistent with the presence of nanoparticles dispersed within residual organic material derived from the leaf extract. At lower magnification (2,000×; Fig. 3B), the overall field revealed numerous irregular, elongated flake- and needle-like structures scattered across the sample surface, reflecting the heterogeneous, aggregated nature of the dried nanoparticle–extract matrix at the micron scale.

Closer examination of an individual aggregate at high magnification (50,000×; Fig. 3C) showed an irregular, rough-textured flake with fine particulate structures adhering to and embedded within its surface, indicating that the nanoparticles were closely associated with the organic (phytochemical) matrix rather than existing as fully free, isolated particles. At intermediate magnification (10,000×; Fig. 3D), several such plate- or sheet-like aggregates of varying size were visible, further confirming the tendency of the biosynthesized particles to cluster into larger irregular aggregates.

Overall, the SEM micrographs indicate that the AgNPs are embedded within, and closely associated with, an organic matrix originating from the *T. erecta* extract, giving rise to an irregular, flake-like aggregate morphology at the micro-scale, while nanoscale particulate features remain discernible at higher magnification. This aggregated surface morphology is consistent with the presence of capping biomolecules noted in the TEM analysis (Section 3.3).

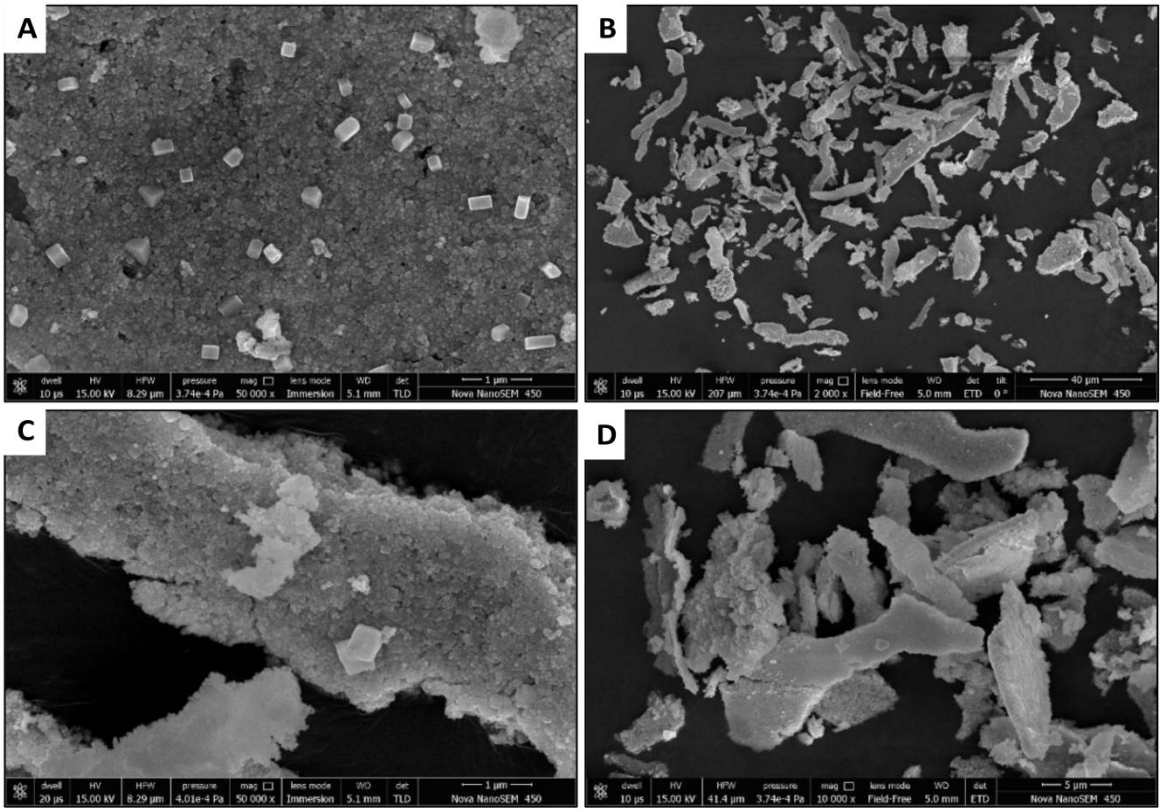


Fig. 3 Scanning electron microscopy (SEM) images of biosynthesized silver nanoparticles at varying magnifications. **(A)** High-magnification (50,000×) view showing distinct, well-dispersed nanoparticles with polygonal/cuboidal morphology (scale bar 1 μm). **(B)** Low-magnification (2,000×) overview showing aggregated flake-like clusters of nanoparticles (scale bar 40 μm). **(C)** Close-up (50,000×) of a nanoparticle aggregate revealing surface texture and embedded crystalline particles (scale bar 1 μm). **(D)** Intermediate magnification (10,000×) view of irregular, plate-like nanoparticle aggregates (scale bar 5 μm).

3.3 Transmission Electron Microscopy (TEM) Analysis of AgNPs

The morphology and size of the biosynthesized AgNPs were further examined by TEM (Fig. 4). The micrograph revealed predominantly spherical to quasi-spherical nanoparticles, with a few particles exhibiting a slightly oval or elongated profile. The particles were largely

polydisperse in nature, ranging from smaller discrete units to comparatively larger particles of roughly similar magnitude to the 20 nm scale marker, with several particles exceeding this dimension. A degree of aggregation and partial fusion between adjacent particles was evident in the micrograph, which is commonly observed in phytosynthesized nanoparticle preparations and has been attributed to the presence of biomolecules from the plant extract acting as capping/stabilizing agents on the nanoparticle surface. A faint, diffuse halo surrounding several particles was also observed, consistent with the presence of this organic capping layer. The particles did not show a sharply faceted crystalline outline under TEM, suggesting the capping biomolecules coat the nanoparticle surface fairly uniformly. The observed particle morphology and aggregation pattern are consistent with the crystalline, nanoscale nature of the AgNPs indicated by the XRD analysis (Section 3.1).

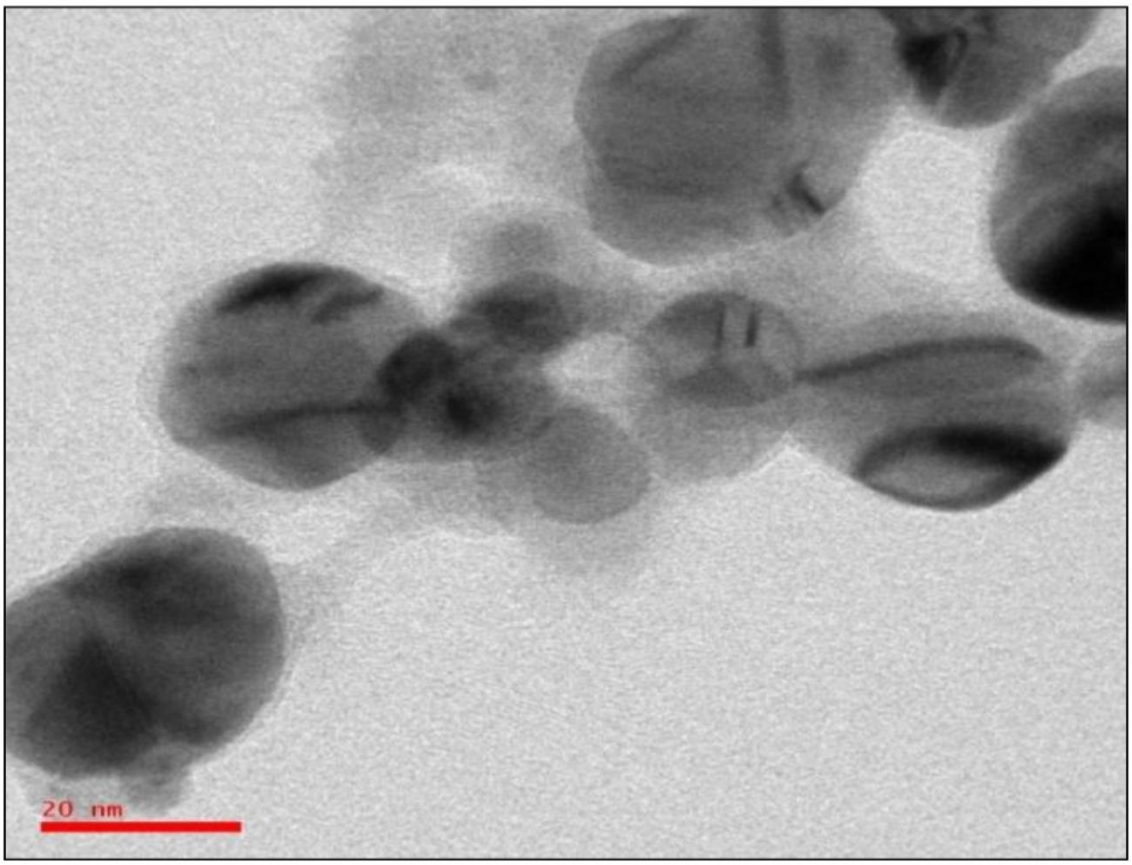


Fig. 4 Transmission electron microscopy (TEM) image of biosynthesized silver nanoparticles showing predominantly spherical to quasi-spherical particles with slight aggregation (scale bar 20 nm).

3.4 In Vitro Antifungal Activity of AgNPs against *Fusarium oxysporum*

The in vitro radial growth assay demonstrated a clear, concentration-dependent and treatment-dependent suppression of *Fusarium oxysporum* mycelial growth across all evaluation intervals (3, 5, and 7 days after inoculation, DAI). The pathogen used in this study was isolated from naturally infected chickpea plants exhibiting characteristic Fusarium wilt symptoms and confirmed by cultural characteristics (Fig. 5), while treatment effects on mycelial growth are presented in Table 1.

The pathogen control (T2, uninoculated with any antifungal agent) exhibited the maximum and unrestricted radial growth at all time points, reaching 36.50 ± 0.25 mm, 69.64 ± 1.13 mm, and 90.00 ± 0.00 mm (full plate coverage) at 3, 5, and 7 DAI, respectively, and was statistically distinct (grouped "a") from all other treatments, validating it as the baseline for calculating percent inhibition. Among the silver nanoparticle (AgNP) treatments, growth suppression increased progressively with concentration. AgNP at 50 ppm (T3) reduced colony diameter to 61.30 mm at 7 DAI, corresponding to 31.89% inhibition, while AgNP at 100 ppm (T4) improved suppression to 46.12 mm (48.76% inhibition). The highest AgNP dose, 200 ppm (T5), achieved substantially greater inhibition (69.27%), restricting growth to 27.66 ± 0.93 mm at 7 DAI, and was statistically at par with Azoxystrobin 80 ppm (T6), both grouped "d," indicating comparable antifungal efficacy at these doses. The standard fungicide treatments outperformed all AgNP concentrations. Azoxystrobin at 80 ppm (T6) inhibited growth by 72.62%, while Azoxystrobin at 100 ppm (T7) produced the strongest suppression among all treatments, limiting colony diameter to just 13.46 ± 0.67 mm at 7 DAI (85.04% inhibition), significantly superior to every other treatment (group "e").

Overall, growth suppression followed the order: T7 > T6 ≈ T5 > T4 > T3 > T2, with all treatment differences statistically significant (CD at P = 0.05: 0.896, 2.695, and 2.286 mm for 3, 5, and 7 DAI, respectively), and low CV values (3.95–6.73%) indicating high experimental precision and reliability of the observed trends.

Table 1 In vitro radial growth (mm) and percent inhibition of *Fusarium oxysporum* mycelium at 3, 5, and 7 days after inoculation (DAI) under different AgNP and Azoxystrobin concentrations, compared with control.

Treatment	3 DAI (Mean ± SE, mm)	5 DAI (Mean ± SE, mm)	7 DAI (Mean ± SE, mm)	Inhibition (%)
T1 Healthy control	0.00 ± 0.00[f]	0.00 ± 0.00 [f]	0.00 ± 0.00 [f]	—
T2 Pathogen	36.50 ± 0.25[a]	69.64 ± 1.13 [a]	90.00 ± 0.00 [a]	0
T3 AgNP 50 ppm	27.08 ± 0.25[b]	48.68 ± 1.29 [b]	61.30 ± 1.11 [b]	31.89
T4 AgNP 100 ppm	20.12 ± 0.41[c]	37.94 ± 0.96 [c]	46.12 ± 1.15 [c]	48.76
T5 AgNP 200 ppm	15.44 ± 0.21[d]	24.32 ± 0.83 [d]	27.66 ± 0.93 [d]	69.27
T6 Azoxystrobin 80 ppm	14.42 ± 0.37 [d]	22.26 ± 0.91 [d]	24.64 ± 0.69 [d]	72.62
T7 Azoxystrobin 100 ppm	8.94 ± 0.44[e]	13.40 ± 0.82 [e]	13.46 ± 0.67 [e]	85.04
CV (%)	3.951	6.733	4.693	
SEm (±)	0.309	0.93	0.789	
SEd (±)	0.437	1.315	1.116	
CD (P=0.05)	0.896	2.695	2.286	

*Means followed by the same superscript are not significantly different according to Tukey's HSD (P = 0.05).

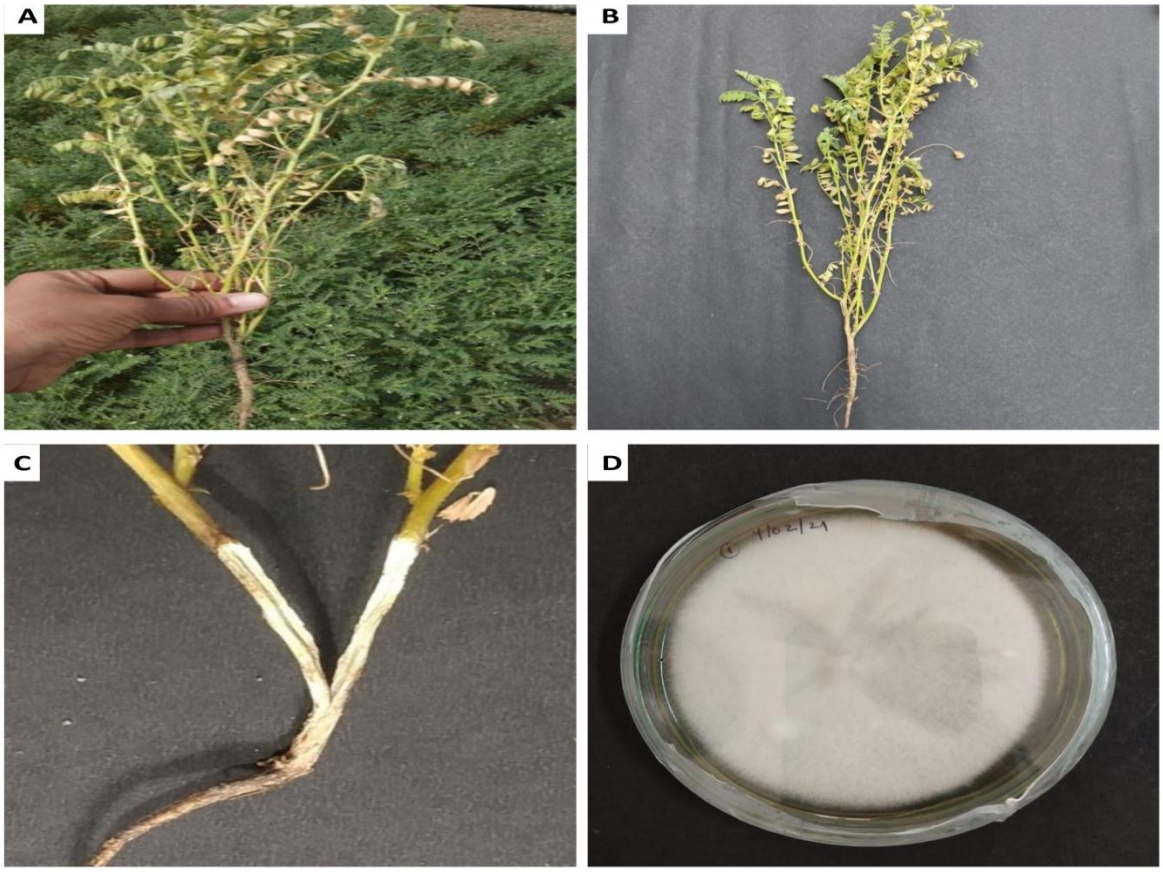


Fig. 5 Symptoms of Fusarium wilt in chickpea and associated pathogen isolation. **(A)** Field symptoms showing wilted, drooping foliage with chlorosis and drying of leaves and pods on an infected plant. **(B)** Uprooted wilted plant showing complete drying of the shoot alongside a comparatively healthier plant. **(C)** Close-up of the stem base/root showing characteristic vascular discoloration associated with *Fusarium* infection. **(D)** Pure culture of *Fusarium oxysporum* f. sp. *ciceris* isolated from infected plant tissue, showing typical white, cottony mycelial growth on culture medium.

3.5 In Vitro Antifungal Activity of AgNPs against *Rhizoctonia solani*

Rhizoctonia solani was isolated from naturally infected chickpea plants exhibiting typical root rot symptoms, including complete drying of plants, root and collar rot, and characteristic brown discoloration of infected tissues. The pathogen was identified based on disease symptoms and its characteristic brown, radiating mycelial growth on potato dextrose agar (PDA) (Fig. 6). The purified culture was subsequently used for evaluating the antifungal efficacy of silver nanoparticles and azoxystrobin under in vitro conditions.

The in vitro assay against *Rhizoctonia solani* revealed a consistent, concentration-dependent reduction in mycelial growth across all treatments and observation intervals (3, 5, and 7

DAI), with a pattern broadly similar to that observed for *Fusarium oxysporum* but with generally higher overall inhibition levels (Table 2). The healthy control (T1) showed no mycelial growth at any time point, confirming freedom from contamination.

The pathogen control (T2) exhibited unrestricted radial growth, reaching 40.42 ± 0.78 mm, 74.86 ± 0.76 mm, and 90.00 ± 0.00 mm (complete plate coverage) at 3, 5, and 7 DAI, respectively, and was statistically distinct from all other treatments (group "a"), serving as the reference for percent inhibition calculations. Among the AgNP treatments, growth suppression rose progressively with increasing concentration. AgNP at 50 ppm (T3) limited growth to 51.98 mm at 7 DAI, yielding 41.49% inhibition. AgNP at 100 ppm (T4) improved suppression further, restricting growth to 35.02 mm (60.67% inhibition), while the highest dose, AgNP 200 ppm (T5), achieved 77.04% inhibition, confining colony diameter to just 20.10 ± 0.64 mm at 7 DAI. Notably, T5 was statistically comparable to Azoxystrobin 80 ppm (T6) at 3 and 5 DAI (both grouped "d"), though the two diverged at 7 DAI, where T6 (16.73 mm, 80.91% inhibition) formed a distinct group ("e"), indicating a slight edge for the fungicide at the later stage.

The fungicide treatments again produced the strongest suppression overall. Azoxystrobin at 100 ppm (T7) was the most effective treatment across all time points, restricting growth to only 7.62 ± 0.45 mm at 7 DAI and achieving the highest inhibition recorded (91.51%), significantly superior to all other treatments (group "f").

Overall, the efficacy ranking was T7 > T6 > T5 > T4 > T3 > T2, with all differences statistically significant (CD at P = 0.05: 1.832, 1.92, and 1.747 mm at 3, 5, and 7 DAI, respectively). CV values (4.20–9.29%) remained within acceptable limits, confirming good experimental reliability, notably with *R. solani* showing marginally greater sensitivity to both AgNP and Azoxystrobin treatments than *F. oxysporum*.

Table 2 In vitro radial growth (mm) and percent mycelial inhibition of *Rhizoctonia solani* at 3, 5, and 7 days after inoculation (DAI) under different AgNP and Azoxystrobin concentrations, compared with control.

Treatment	**3 DAI (Mean ± SE, mm)**	**5 DAI (Mean ± SE, mm)**	**7 DAI (Mean ± SE, mm)**	**Mycelial inhibition (%)**
T1 Healthy control	0.00 ± 0.00^{f}	0.00 ± 0.00^{f}	0.00 ± 0.00^{g}	—
T2 Pathogen	40.42 ± 0.78^{a}	74.86 ± 0.76^{a}	90.00 ± 0.00^{a}	0

T3 AgNP 50 ppm	23.20 ± 0.66[b]	41.56 ± 0.80 [b]	51.98 ± 1.02 [b]	41.49
T4 AgNP 100 ppm	16.56 ± 0.87[c]	28.38 ± 0.75 [c]	35.02 ± 0.88 [c]	60.67
T5 AgNP 200 ppm	11.54 ± 0.80[d]	17.58 ± 0.83 [d]	20.10 ± 0.64 [d]	77.04
T6 Azoxystrobin 80 ppm	9.62 ± 0.50 [d]	14.66 ± 0.64 [d]	16.73 ± 0.81[e]	80.91
T7 Azoxystrobin 100 ppm	5.18 ± 0.35[e]	8.06 ± 0.44 [e]	7.62 ± 0.45 [f]	91.51
CV (%)	9.293	5.604	4.2	
SEm (±)	0.632	0.663	0.594	
SEd (±)	0.894	0.937	0.84	
CD (P=0.05)	1.832	1.92	1.747	

*Means followed by the same superscript are not significantly different according to Tukey's HSD (P = 0.05).



Fig. 6 Symptoms of root rot in chickpea caused by *Rhizoctonia solani* and associated pathogen isolation. **(A)** Field symptom showing complete drying and blighting of the plant with straw-coloured, dried foliage and pods. **(B)** Infected plant in the field showing white mycelial growth colonizing the lower stem and root region. **(C)** Close-up of the affected

root/collar region showing brown discoloration and rotting of tissue. **(D)** Pure culture of *Rhizoctonia solani* isolated from infected roots, showing characteristic brown, radiating mycelial growth with a central white tuft on culture medium.

3.6 In Vivo Antifungal Efficacy of AgNPs under Pot Conditions

The in vivo evaluation of disease severity, based on the 0–5 disease rating scale expressed as percent disease index (PDI) at 60 days after sowing, demonstrated that AgNP and Azoxystrobin treatments significantly reduced disease incidence caused by both *Fusarium oxysporum* f. sp. *ciceris* and *Rhizoctonia solani* compared to the untreated pathogen control, with a dose-dependent trend consistent with the in vitro findings (Table 3).

The healthy control recorded no disease symptoms (0.0 ± 0.00) for either pathogen, while plants inoculated with the pathogen alone and left untreated showed the highest disease severity, at 90.0 ± 2.00 for *F. oxysporum* and 88.0 ± 2.00 for *R. solani*, both forming a statistically distinct group ("a") and serving as the baseline for calculating percent disease reduction.

Among the AgNP treatments, disease severity declined progressively with increasing concentration. AgNP at 50 ppm reduced disease severity to 58.4 ± 3.31 (35.1% reduction) against *F. oxysporum* and 54.0 ± 2.83 (38.6% reduction) against *R. solani*. AgNP at 100 ppm improved efficacy further, lowering severity to 46.0 ± 2.76 (48.9% reduction) and 35.2 ± 2.73 (60% reduction) for the two pathogens, respectively. The highest AgNP dose, 200 ppm, achieved the greatest suppression among nanoparticle treatments, reducing disease severity to 31.6 ± 2.93 (64.9% reduction) for *F. oxysporum* and 24.4 ± 2.14 (72.3% reduction) for *R. solani*, and was statistically at par with Azoxystrobin 80 ppm (both grouped "d") for both pathogens.

The standard fungicide treatments again provided the strongest disease control. Azoxystrobin at 80 ppm reduced disease severity by 68.4% and 75% for *F. oxysporum* and *R. solani*, respectively, while Azoxystrobin at 100 ppm was the most effective treatment overall, achieving 84.4% and 86.4% disease reduction, with severity values of only 14.0 ± 2.10 and 12.0 ± 1.41, respectively (group "e"), significantly superior to all other treatments.

Overall, the efficacy trend under in vivo conditions mirrored the in vitro results, following the order Azoxystrobin 100 ppm > Azoxystrobin 80 ppm ≈ AgNP 200 ppm > AgNP 100 ppm > AgNP 50 ppm > pathogen control, with all differences statistically significant (CD at 5% = 6.9 and 5.8 for *F. oxysporum* and *R. solani*, respectively), and *R. solani* again showing marginally greater sensitivity to all treatments than *F. oxysporum*.

Table 3 In vivo disease severity (0–5 scale, PDI) and percent disease reduction in chickpea against *Fusarium oxysporum* f. sp. *ciceris* and *Rhizoctonia solani* at 60 days after sowing under AgNP and Azoxystrobin treatments.

Treatment	***Fusarium Oxysporum* fsp *ciceris***		***Rhizoctonia solani***	
	Mean ± SE	**Disease reduction (%)**	**Mean ± SE**	**Disease reduction (%)**
Control	0.0 ± 0.00[f]		0.0 ± 0.00 [f]	
Pathogen only	90.0 ± 2.00[a]		88.0 ± 2.00 [a]	
AgNP 50 ppm	58.4 ± 3.31[b]	35.1	54.0 ± 2.83 [b]	38.6
AgNP 100 ppm	46.0 ± 2.76[c]	48.9	35.2 ± 2.73[c]	60
AgNP 200 ppm	31.6 ± 2.93[d]	64.9	24.4 ± 2.14[d]	72.3
Azoxystrobin 80 ppm	28.4 ± 2.04[d]	68.4	22.0 ± 1.41[d]	75
Azoxystrobin 100 ppm	14.0 ± 2.10[e]	84.4	12.0 ± 1.41[e]	86.4
SEm (±)	2.38		2	
CD (LSD) at 5%	6.9		5.8	
SE(d)	3.37		2.83	
Tukey HSD (5%)	9.62		8.97	

*Means followed by the same superscript are not significantly different according to Tukey's HSD (P = 0.05).

4. Discussion

The present study demonstrates that aqueous *Tagetes erecta* flower extract can efficiently reduce Ag^+ ions into crystalline, nanoscale AgNPs that possess dose-dependent, near-fungicide-equivalent activity against two economically important chickpea soil-borne pathogens. These findings both corroborate and extend the existing literature on marigold-mediated nanoparticle biosynthesis and phyto-synthesized antifungal nanomaterials more broadly.

The XRD reflections obtained in this study, indexable to the (111) and (200) planes of face-centred cubic metallic silver, are consistent with earlier reports on *T. erecta*-derived AgNPs, in which comparable Bragg peaks and a crystallite growth preference along the (111) plane were confirmed by high-resolution TEM [9]. The 19 nm crystallite size calculated here also aligns closely with the nanoscale dimensions reported for other marigold-based syntheses,

including the 10–15 nm particles obtained by Burlec et al. (2022) using aqueous and ethanolic *T. erecta* extracts, and the earlier characterization of marigold-flower AgNPs by Padalia et al. (2015). The additional reflections attributable to a minor AgCl phase are a frequently reported feature of plant-mediated silver nanoparticle synthesis, arising from chloride ions naturally present in floral tissue that compete with reducing biomolecules for available Ag^{+}; similar Ag/AgCl composite phases have been documented in extracts of Jatropha seed, macadamia nutshell xylan, argan press-cake saponins, and Chara algae, where the relative proportion of the two phases was shown to depend on extract pH and chloride availability during synthesis. Since AgCl itself possesses recognized antimicrobial and photocatalytic activity, its co-formation in the present system is unlikely to have compromised, and may even have marginally reinforced, the overall antifungal performance of the nanoparticle preparation.

The SEM and TEM observations of predominantly spherical to quasi-spherical particles embedded within an organic phytoconstituent matrix are typical of biogenic AgNPs and reflect the dual reducing–capping role of flavonoid, terpenoid, and phenolic constituents abundant in *T. erecta* [6,8]. The aggregation and partial fusion of particles observed here has likewise been reported for other floral and leaf extract-mediated syntheses and is generally attributed to residual biomolecules coating the nanoparticle surface, which, while promoting colloidal stability, can also modestly reduce the effective surface area available for antimicrobial ion release [12].

The dose-dependent inhibition of *F. oxysporum* and *R. solani* mycelial growth observed in vitro is mechanistically consistent with the well-documented multi-target mode of action of AgNPs against phytopathogenic fungi. AgNPs are known to adsorb onto and permeabilize the fungal cell wall and plasma membrane, generate reactive oxygen species that damage lipids, proteins and DNA, and interfere with mitochondrial and ribosomal function, collectively producing hyphal shrinkage, vacuolation, and leakage of cytoplasmic contents [12,13]. Comparable transcriptomic and ultrastructural evidence in *Fusarium graminearum* [14] and in the *Fusarium solani* species complex [15] has shown that AgNP exposure disrupts cellular energy metabolism, elevates intracellular reactive oxygen species, and induces oxidative-stress-responsive gene expression, while genome-wide transcriptomic analysis in the rice false smut pathogen *Ustilaginoidea virens* further indicates that AgNPs can alter chromatin-level gene regulation in addition to direct structural damage [16]. These findings reinforce that the inhibition recorded in the present poisoned-food assay likely reflects similar sub-

lethal and lethal cellular damage rather than a single-target effect. The progressive rise in inhibition from 50 to 200 ppm mirrors the concentration-dependent trends reported for AgNPs synthesized from Avena fatua against *F. oxysporum f. sp. lycopersici* [4], *Solanum nigrum* against *Fusarium circinatum* [5], *Hyssopus/Salvia officinalis* extracts against Fusarium spp. [17], and guava leaf extract against *Colletotrichum capsici* [18], collectively supporting the generalizability of dose-dependent AgNP antifungal efficacy across diverse plant-mediated synthesis systems and fungal targets. A comprehensive four-pathogen screen of *Azadirachta indica*-derived AgNPs likewise recorded substantial, though pathogen-variable, inhibition of *R. solani* alongside near-complete suppression of *Sclerotinia sclerotiorum* and *Colletotrichum falcatum*, underscoring that AgNP efficacy against *R. solani* specifically is reproducible across independent green-synthesis platforms [19].

Notably, *R. solani* was consistently more sensitive to both AgNPs and azoxystrobin than *F. oxysporum* at equivalent concentrations in the present study. This differential susceptibility may reflect underlying differences in cell wall architecture between the two pathogens; *R. solani*, a basidiomycete lacking the pentaketide melanin biosynthetic pathway in several anastomosis groups, possesses a comparatively thinner, glucan/mannan-rich wall relative to the chitin-reinforced, often melanized structures of many ascomycetes, potentially rendering it more permeable to nanoparticle penetration and silver ion influx. This interpretation is consistent with direct comparative work showing that *R. solani* exhibits markedly lower tolerance to silver nanoparticle exposure than the more robust, melanized biocontrol fungus *Trichoderma harzianum* [20], and aligns with reports of AgNPs derived from Bacillus megaterium-synthesized selenium nanoparticle systems achieving strong in vitro and in vivo suppression of *R. solani* in faba bean [21]. Together, these observations add a pathogen-specific dimension to the growing literature on AgNP efficacy and suggest that dose optimization for integrated disease management may need to be pathogen-tailored rather than uniform.

The near-parity of 200 ppm AgNPs with azoxystrobin 80 ppm, both in vitro and under pot conditions, is agriculturally significant, particularly given that the single-site mode of action of QoI fungicides such as azoxystrobin, which inhibit electron transfer at the Qo site of the mitochondrial cytochrome bc1 complex, carries an inherently high risk of resistance development through target-site mutations such as the widely reported G143A substitution in fungal cytochrome b [22]. This resistance risk strengthens the rationale for developing AgNP-based alternatives with multi-target modes of action that are less prone to single-mutation

escape. Comparable nano-based protection has been reported for chickpea itself: silver nanoparticles biosynthesized using rhizospheric microflora of chickpea significantly reduced in vivo wilt severity caused by *F. oxysporum* f. sp. ciceris [23], ZnO nanoparticle seed priming reduced Fusarium wilt incidence by up to 90% relative to untreated controls [24], while thiamine-loaded chitosan nanoparticles have similarly been shown to enhance wilt resistance and stimulate growth in chickpea [25]. Together with the present findings, this body of work positions phytosynthesized metal nanoparticles as a credible complement to, rather than outright replacement for, conventional strobilurin fungicides, potentially enabling reduced-dose integrated programmes that lower environmental and resistance-selection pressure. Nevertheless, the somewhat lower efficacy of AgNPs relative to azoxystrobin 100 ppm, together with the unresolved questions of soil silver persistence, non-target microbiota effects, and phytotoxicity at higher application rates, underscores that field-scale validation and formal risk assessment remain necessary before large-scale deployment of *T. erecta*-mediated AgNPs in chickpea disease management programmes.

5. Conclusion

The present study demonstrates the successful green synthesis of crystalline, spherical to quasi-spherical AgNPs (~20 nm) using *Tagetes erecta* flower extract, characterized by fcc metallic silver reflections (2θ = 38.1°, 46.2°) alongside a minor AgCl phase, and stabilized by a phytoconstituent capping layer evident from SEM/TEM morphology. The synthesized AgNPs exhibited pronounced, concentration-dependent antifungal activity against both *F. oxysporum* and *R. solani*, with 200 ppm producing the strongest suppression in vitro (69.27% and 77.04% mycelial inhibition, respectively) and in vivo (64.9% and 72.3% disease reduction), performing statistically at par with azoxystrobin at 80 ppm across both pathosystems. *R. solani* consistently showed greater sensitivity to AgNP treatment than *F. oxysporum* at equivalent concentrations, indicating pathogen-specific variation in susceptibility. While azoxystrobin at 100 ppm retained the highest overall efficacy (85.04–91.51% in vitro; 84.4–86.4% in vivo), the near-fungicide-equivalent performance of 200 ppm AgNPs highlights their potential as a sustainable, low-toxicity alternative or complementary strategy to chemical fungicides in managing Fusarium wilt and Rhizoctonia root rot. These findings support the further development of phytosynthesized AgNPs as a viable component of integrated disease management, though field-scale validation, dose optimization, and phytotoxicity/non-target safety assessments are warranted before practical deployment.

Author contributions

V.G. wrote the main manuscript text with the help of P.P. and A.C. A.K. led the project and designed the experiments. All authors contributed to the experimental work. A.K. and V.G. were involved in data analysis. P.P. prepared the figures and led the characterization studies. V.G. conducted the antifungal bioassays. R.S. and A.C. assisted with sample collection and processing. All authors reviewed the manuscript.

Funding

The authors declare that no funding was received for this study.

Data availability

The datasets generated and analysed during the current study are available from the corresponding author on reasonable request.

Declarations

Ethics approval and consent to participate

The study was conducted in compliance with institutional, national, and international guidelines. No protected or endangered plant species were involved, and no special permits were required for collection.

Consent for publication

Not applicable.

Competing interests

The authors declare no competing interests.

Acknowledgements

The authors are thankful to the Malaviya National Institute of Technology (MNIT), Jaipur, for providing the characterization facilities used in this study.

References

1. Navas-Cortés, J. A., Hau, B., & Jiménez-Díaz, R. M. (2000). Yield loss in chickpeas in relation to development of Fusarium wilt epidemics. *Phytopathology*, *90*(11), 1269-1278.

2. Al-Sahli, S. A., Al-Otibi, F., Alharbi, R. I., Amina, M., & Al Musayeib, N. M. (2024). Silver nanoparticles improve the fungicidal properties of *Rhazya stricta decne* aqueous extract against plant pathogens. *Scientific Reports*, *14*(1), 1297.

3. Gautam, V., Garg, V., Meena, N., Dashrath, H. A., Singh, K., Kumar, A., ... & Singh, R. K. (2025). Fungal-derived ZnO nanoparticles functionalized with riboflavin and UDP-GlcNAc exhibit potent nematicidal activity against M. incognita. *Scientific Reports*, *15*(1), 38427.

4. Qureshi, A. K., Farooq, U., Shakeel, Q., Ali, S., Ashiq, S., Shahzad, S., Nazir, M. T., Seleiman, M. F., Jamal, A., Saeed, M. F., & Manachini, B. (2023). The green synthesis of silver nanoparticles from Avena fatua extract: Antifungal activity against *Fusarium oxysporum f.sp. lycopersici*. Pathogens, 12(10), 1247. https://doi.org/10.3390/pathogens12101247

5. Abd-Elhamed, W., Mohamed, A. A., Saad, Z. H., Hassanien, S. E. S. I., Salem, M. Z., & El-Hefny, M. (2025). Green synthesis of silver nanoparticles mediated by *Solanum nigrum* leaf extract and their antifungal activity against pine pathogens. *Scientific Reports*, *15*(1), 35025.

6. Padalia, H., Moteriya, P., & Chanda, S. (2015). Green synthesis of silver nanoparticles from marigold flower and its synergistic antimicrobial potential. Arabian Journal of Chemistry, 8(5), 732–741. https://doi.org/10.1016/j.arabjc.2014.11.015

7. Singh, R. K., Priyadarshini, A., Yeam, D. A., Bhattacharya, A., Vaishnav, R., & Kumar, A. (2025). Green synthesis of silver nanoparticles using marigold flowers extract for eco-friendly management of root knot nematode. *Plant Nano Biology*, *12*, 100150.

8. Burlec, A. F., Hăncianu, M., Macovei, I., Mircea, C., Fifere, A., Turin-Moleavin, I. A., ... & Corciovă, A. (2022). Eco-friendly synthesis and comparative in vitro biological evaluation of silver nanoparticles using *Tagetes erecta* flower extracts. *Applied Sciences*, *12*(2), 887.

9. Zarate-Escobedo, J., Zavaleta-Mancera, H. A., Soto-Hernández, R. M., Pérez-Rodríguez, P., Vilchis-Nestor, A. R., Silva-Rojas, H. V., & Trejo-Téllez, L. I. (2024). Long-lasting silver nanoparticles synthesized with *Tagetes erecta* and their antibacterial activity against Erwinia amylovora, a serious rosaceous pathogen. Plants, 13(7), 981. https://doi.org/10.3390/plants13070981

10. Jain, S., & Mehata, M. S. (2017). Medicinal plant leaf extract and pure flavonoid mediated green synthesis of silver nanoparticles and their enhanced antibacterial property. *Scientific reports*, *7*(1), 15867.

11. Nene, Y. L., Haware, M. P., & Reddy, M. V. (1981). *Chickpea diseases: Resistance-screening techniques* (Information Bulletin No. 10). International Crops Research Institute for the Semi-Arid Tropics (ICRISAT), Patancheru, India.

12. Matras, E., Gorczyca, A., Przemieniecki, S. W., & Oćwieja, M. (2022). Surface properties-dependent antifungal activity of silver nanoparticles. Scientific Reports, 12, 18046. https://doi.org/10.1038/s41598-022-22659-2

13. Li, L., Pan, H., Deng, L., Qian, G., Wang, Z., Li, W., & Zhong, C. (2022). The antifungal activity and mechanism of silver nanoparticles against four pathogens causing kiwifruit post-harvest rot. Frontiers in Microbiology, 13, 988633. https://doi.org/10.3389/fmicb.2022.988633

14. Jian, Y., Chen, X., Ahmed, T., Shang, Q., Zhang, S., Ma, Z., & Yin, Y. (2022). Toxicity and action mechanisms of silver nanoparticles against the mycotoxin-producing fungus *Fusarium graminearum*. Journal of Advanced Research, 38, 1–12. https://doi.org/10.1016/j.jare.2021.09.006

15. Shen, T., Wang, Q., Li, C., Zhou, B., Li, Y., & Liu, Y. (2020). Transcriptome sequencing analysis reveals silver nanoparticles antifungal molecular mechanism of the soil fungi Fusarium solani species complex. *Journal of hazardous materials*, *388*, 122063.

16. Wen, H., Shi, H., Jiang, N., Qiu, J., Lin, F., & Kou, Y. (2023). Antifungal mechanisms of silver nanoparticles on mycotoxin producing rice false smut fungus. iScience, 26(1), 105763. https://doi.org/10.1016/j.isci.2022.105763

17. Dėnė, L., Chrapačienė, S., Laurinaitytė, G., Rudinskaitė, A., Viškelis, J., Viškelis, P., & Balčiūnaitienė, A. (2024). Green synthesis of silver nanoparticles with *Hyssopus officinalis* and *Salvia officinalis* extracts, their properties, and antifungal activity on Fusarium spp. Plants, 13(12), 1611. https://doi.org/10.3390/plants13121611

18. Mazhar, S., Hyder, S., Khan, B. S., Gondal, A. S., Ahmed, R., Iqra, & Iqbal, M. (2025). Green synthesis of silver nanoparticles using guava leaves: an effective strategy to control chilli fruit rot disease. BMC Plant Biology, 25(1), 499. https://doi.org/10.1186/s12870-025-06528-4

19. Singh, J., Kumar, A., Nayal, A. S., Vikal, S., Shukla, G., Singh, A., Singh, A., Goswami, S., Kumar, A., Gautam, Y. K., Verma, Y., Gaurav, S. S., & Pratap, D. (2024). Comprehensive

antifungal investigation of green synthesized silver nanoformulation against four agriculturally significant fungi and its cytotoxic applications. Scientific Reports, 14, 5934. https://doi.org/10.1038/s41598-024-56619-9

20. Oktarina, H., Mukhriza, T., Šiller, L., & Singleton, I. (2022). Differential tolerance of *Trichoderma harzianum* and *Rhizoctonia solani* towards silver nanoparticles: potential for agricultural applications? Jurnal Natural, 22(2), 73–77. https://doi.org/10.24815/jn.v22i2.24149

21. Hashem, A. H., Abdelaziz, A. M., Askar, A. A., Fouda, H. M., Khalil, A. M. A., Abd-Elsalam, K. A., & Khaleil, M. M. (2021). Bacillus megaterium-mediated synthesis of selenium nanoparticles and their antifungal activity against *Rhizoctonia solani* in faba bean plants. Journal of Fungi, 7(3), 195. https://doi.org/10.3390/jof7030195

22. Fernández-Ortuño, D., Torés, J. A., de Vicente, A., & Pérez-García, A. (2008). Mechanisms of resistance to QoI fungicides in phytopathogenic fungi. International Microbiology, 11(1), 1–9.

23. Kaur, P., Thakur, R., Duhan, J. S., & Chaudhury, A. (2018). Management of wilt disease of chickpea in vivo by silver nanoparticles biosynthesized by rhizospheric microflora of chickpea (*Cicer arietinum*). Journal of Chemical Technology & Biotechnology, 93(11), 3233–3243. https://doi.org/10.1002/jctb.5680

24. Farhana, F., Munis, M. F. H., Alamer, K. H., Althobaiti, A. T., Kamal, A., Liaquat, F., Haroon, U., Ahmed, J., Chaudhary, H. J., & Attia, H. (2022). ZnO nanoparticle-mediated seed priming induces biochemical and antioxidant changes in chickpea to alleviate Fusarium wilt. Journal of Fungi, 8(7), 753. https://doi.org/10.3390/jof8070753

25. Muthukrishnan, S., Murugan, I., & Selvaraj, M. (2019). Chitosan nanoparticles loaded with thiamine stimulate growth and enhances protection against wilt disease in chickpea. Carbohydrate Polymers, 212, 169–177. https://doi.org/10.1016/j.carbpol.2019.02.037